DOI: 10.24996/ijs.2025.66.11.21

ISSN: 0067-2904

Structural and Dielectric Properties of Mn Doped SnO_2 Prepared by Solid State Reaction

Sara S. Mahmood[1], Bushra A. Hasan[2], Aws F. Rauuf [1*], Ahmad A. Hasan [2]
[1]*Scientific Research Commission, Baghdad, Iraq.*
[2]*Department of Physics, College of Science, University of Baghdad, Baghdad, Iraq.*

Received: 18/3/2024 Accepted: 27/10/2024 Published: 30/11/2025

Abstract

This study shows how the structural and dielectric properties of $(SnO_2)_{1-x}(Mn_2O_3)_x$, (where x=0.00, 0.03, 0.05,0.07, and 0.09) prepared using the solid state reaction technique, are affected by the doping of semiconducting metal oxide Mn_2O_3. Structural analysis of the composites was carried out using information from the composite samples obtained from X-ray diffraction (XRD). The diffraction peak shifting in XRD patterns indicated that Mn ions were successfully incorporated into the SnO_2 crystal lattice. Mn ions were successfully doped in the Tin oxide matrix lattice with the subsequent increase of doping levels. The average crystal size evaluated using Scherrer's equation was found to vary from 33 to 37 nm, and the lattice constants were a=4.68-3.69 and c=3.166-3.173. This work also tested the dielectric characteristics of $(SnO_2)_{1-x}(Mn_2O_3)_x$ composites. The effects of Mn doping were interpreted and discussed. The effects of Mn doping on the $\sigma_{a.c}(\omega)$, exponent (s), dielectric constant, dielectric loss, relaxation time, and polarizability were also studied.

Keywords - Mn doped SnO_2, XRD, A.C conductivity, dielectric constants

الخصائص التركيبية والعزلية لثاني أوكسيد القصدير المشوب بالمنغنيز والمحضر بتفاعل الحالة الصلبة

سارة صادق محمود[1] ، بشرى عباس حسن[2] ، اوس فيصل رؤوف[1*] ، احمد عباس حسن[2]
[1] هيئة البحث العلمي، بغداد، العراق.
[2] قسم الفيزياء ، كلية العلوم ، جامعة بغداد ، بغداد ، العراق .

الخلاصة:

تستعرض هذه الدراسة كيفية تأثر الخواص التركيبية والعزلية لمتراكبات $(SnO_2)_{1-x}(Mn_2O_3)_x$ (حيث ان قيم x=0.00, 0.03, 0.05,0.07, 0.09) عند التشويب بالمنغنيز، والتي حضرت بتقنية تفاعل الحالة الصلبة . تم تحليل التركيب الهيكلي لنماذج المتراكبات من المعلومات المتحصلة من تقنية حيود الاشعة السينية . اشار الزحف في قمة الطيف للأشعة السينية الى ان عملية تطعيم الشبيكة البلورية لأوكسيد القصدير بأيونات المنغنيز قد تمت بنجاح. ان تطعيم المادة المضيفة وهي اوكسيد القصدير بأيونات المنغنيز تمت بتتابع مع زيادة مستويات التطعيم. ان معدل الحجم البلوري المحسوب باستخدام معادلة شيرر يتراوح بين (33 الى 37) نانومتر وثابت الشبيكة يتراوح بين a=4.68−3.69 بينما c=3.166−3.173. كذلك في هذا البحث تم فحص الخصائص العزلية لمتراكبات $(SnO_2)_{1-x}(Mn_2O_3)_x$. قمنا بتفسير ومناقشة آثار

*Email: aws.raouf1104@sc.uobaghdad.edu.iq

تشويب المنغنيز على $\sigma_{a.c}(\omega)$ و العامل الاسي (s) ,ثابت العزل ، معامل الفقد ، زمن الاسترخاء و الاستقطابية.

Introduction

In recent years, many reports on wide-band semiconductors have been published, primarily due to their numerous applications in optical devices [1]. Tin oxide (SnO_2) is an n-type semiconductor material with a large exciton binding energy of 130 MeV and a wide band gap of 3.6 eV. It can be used for Diluted Magnetic Semiconductor (DMS) materials [2,3]. Owing to their high thermal solubility (10 mol%), Mn ions may be a suitable substitute for Sn ions in SnO_2 lattices. This would enhance the injected spin and carrier values, making Mn-doped SnO_2 a promising candidate for spintronics applications [4,5]. until now, most research has focused on examining the magnetic characteristics of SnO_2 doped with Mn. [6,7]. However, further studies investigating the dielectric characteristics of Mn-doped SnO_2 are needed, and should be carried out. Numerous techniques, including the sol-gel approach, chemical co-precipitation method, chemical precipitation method, and others, are used to manufacture doped SnO_2. It is anticipated that varying Mn concentrations in SnO_2 may impact its optical, electrical, and structural characteristics. As far as is currently known, relatively few studies have addressed how the Mn dopant concentration affects the structural and dielectric characteristics.

The main topics of this work are the production of $(SnO_2)_{1-x}(Mn_2O_3)_x$ composites and the investigation of the effects of Mn doping ratios on the structural and electrical properties.

Experimental

Solid state reaction approach was used to prepare $(SnO_2)_{1-x}(Mn_2O_3)_x$ composites (x=0, 3%, 5%, 7%, and 9%). Alfa Aesar's, 99.99% purity SnO_2 and Mn_2O_3 powders were combined in the proper proportion. The mixture was sintered in air for one hour at 1000ºC. The powder was then extracted and compressed at 6 bar to create dense pellets of 12mm diameter.

The pellets' structural investigation was undertaken using an X-ray diffractometer (Siemens, D5000) with a Cu-Kα(λ=1.544A˚) source. The dielectric characteristics were measured using an LRC meter (GW Instek LCR-8201, V= 0.1-1.3 Volt, F=12 Hz-200 KHz).
The following formula was used to determine the prepared samples' lattice constant:

$$\frac{1}{d^2} = \frac{h^2 + l^2}{a^2} + \frac{k^2}{c^2} \quad (1)$$

Using Scherrer's formula, the crystal size of $(SnO_2)_{1-x}(Mn_2O_3)_x$ composites was computed [8]:

$$D = \frac{0.98\lambda}{\beta \cos\theta} \quad (2)$$

Where: θ is the diffraction angle, λ is the X-ray wavelength (1.54 Å), and β is the Full Width at Half Maximum (FWHM) of the XRD peaks.
The following relation was used to calculate conductivity (σ_{ac}):

$$\sigma_{ac} = \varepsilon_0 \varepsilon_1 \omega \tan\delta \quad (3)$$

where: $\omega = 2\pi f$ is the angular frequency, ε_1 is real dielectric constant, and ε_0 is the permittivity of free space. The hopping conduction process is what causes the conductivity to arise [9]. In general, frequency dependent conductivity can be expressed as:

$$\sigma(\omega,T)=\sigma_{dc}(T)+a(T)\omega^s \quad (4)$$

Where the first component $\sigma_{dc}(T)$ is temperature dependent, and the correlation of the hopping mechanism is found in the second part $a(T)\omega^s$, which is the power of angular frequency.
The dielectric constant and dielectric loss were measured by applying the following relations [10]:

$$\varepsilon_1= C \cdot t / \varepsilon_0 \cdot A \quad (5)$$

Where: ε_1 is the real dielectric constant, C is the capacitance, A is the effective area and t is the thickness of the sample.
The imaginary dielectric constant (ε_2) was calculated according to:

$$\varepsilon_2= \sigma_{ac}/ \omega \varepsilon_o \quad (6)$$

Results and Discussion

The crystal structure studies of $(SnO_2)_{1-x}(Mn_2O_3)_x$ composites were investigated using an X-ray spectrophotometer, and the XRD patterns were obtained. The XRD patterns of $(SnO_2)_{1-x}(Mn_2O_3)_x$ composites for the different values of x are displayed in Figure 1. The appearance of several diffracted peaks predicted the produced materials' polycrystalline composition. The sample's crystal structure displayed three dominant peaks, with positions at $2\theta=26.4^o$, 34.21^o, 38.24^o, and 52.09^o for the peaks (110), (101), (201), and (211), respectively. The diffraction peaks were consistent with the rutile-type tetragonal structure of SnO_2 data from the JCPDS standard (No. 88-0287). The distinct diffraction peaks clearly indicated the well-crystallized state of the $(SnO_2)_{1-x}(Mn_2O_3)_x$ composites. When the doping ratio is high, a small diffraction peak related to manganese is seen in the XRD patterns. When the Mn content increased, the diffraction peaks shifted towards higher angles, indicating that the Mn ions had replaced the Sn sites without altering the rutile structure.

The least squares approach was used to get the XRD peak positions, as shown in Table 2. Lattice characteristics decreased when the composites' Mn concentration rose to 7%. The reduced ionic radius of Mn^{3+} (0.65 Å) site, which is substituted for Sn^{4+} (0.69 Å) site, may be the cause of the lattice constant shrinkage [11]. The crystallite size of the $(SnO_2)_{1-x}(Mn_2O_3)_x$ composites are displayed in Table 1. The produced composites had crystallite sizes that ranged from 33 to 37 nm on average. The average crystallite size of the composites was seen to rise at low Mn content ($x<0.07$) and to decrease at high Mn content ($x>0.07$). Crystal size may decrease as a result of a reduction in the diffusion rate brought on by an increase in the rate of dopants' atoms. It was found that when SnO_2 is doped with Mn, a certain concentration of Mn atoms may prefer to position close to or at crystal boundary regions. This could inhibit the crystals from growing during the process, hence reducing the size of the crystallites [12]. Many researchers have noted that an increase in Mn concentration causes a reduction in crystal size [13].

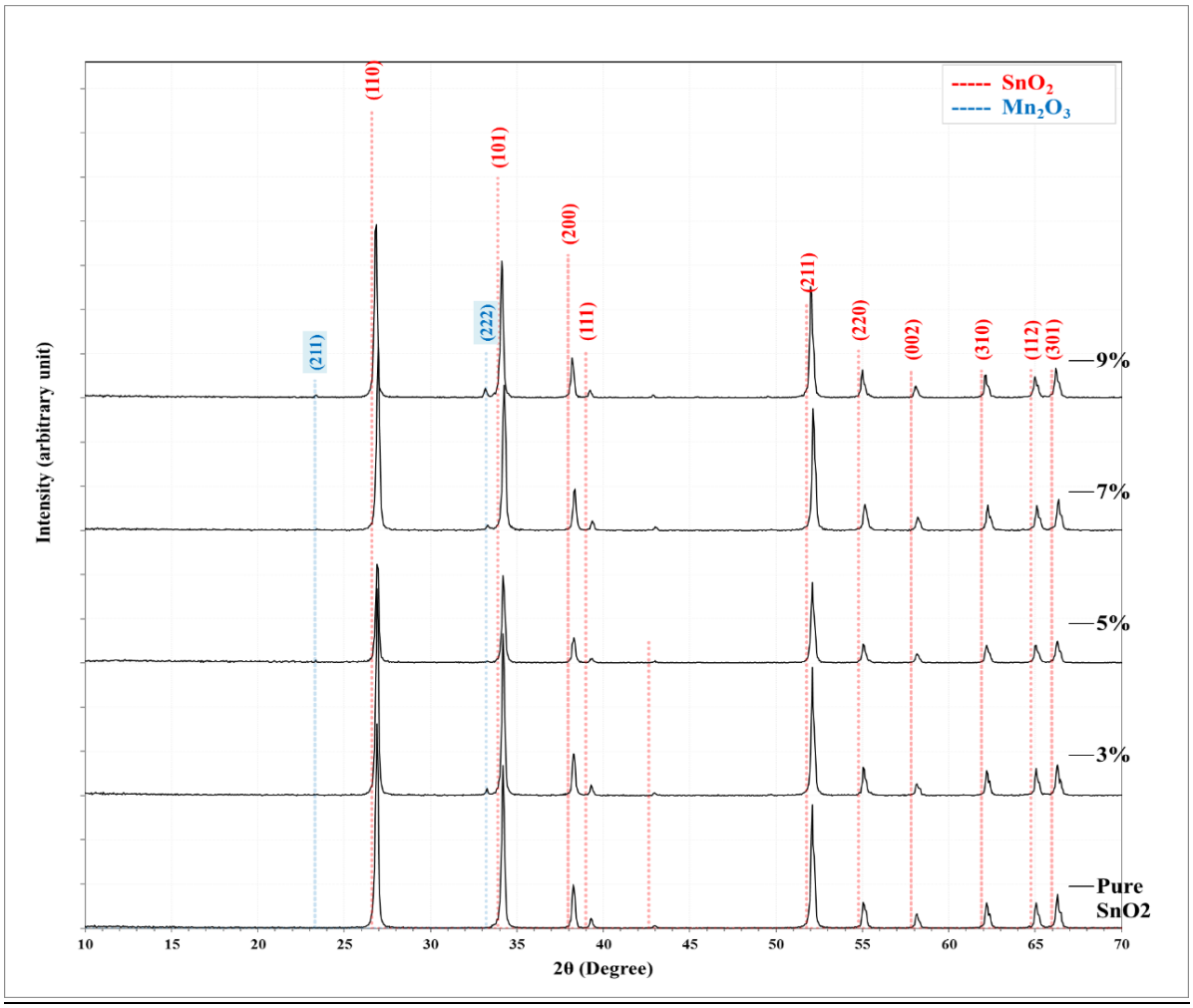

Figure 1: X-ray diffraction of $(SnO_2)_{1-x}(Mn_2O_3)_x$ composites.

Table 1: X-ray diffraction data of $(SnO_2)_{1-x}(Mn_2O_3)_x$ composites.

Mn2O3%	2θ (Deg.)	FWHM (Deg.)	d_{hkl} (Å)	C.S (nm)	hkl	Phase
Pure	26.91	0.2434	3.3109	33.6	(110)	SnO_2
	34.21	0.1894	2.6189	43.9	(101)	SnO_2
	38.24	0.2435	2.3516	34.5	(200)	SnO_2
	39.27	0.2434	2.2924	34.7	(111)	SnO_2
	52.09	0.2975	1.7543	29.7	(211)	SnO_2
	55.04	0.3246	1.6671	27.6	(220)	SnO_2
	58.15	0.2975	1.5851	30.6	(002)	SnO_2
	62.21	0.2976	1.4911	31.2	(310)	SnO_2
	65.02	0.3246	1.4332	29.0	(112)	SnO_2
	66.29	0.3516	1.4088	27.0	(301)	SnO_2
3	26.91	0.2164	3.3109	37.8	(110)	SnO_2
	34.21	0.1894	2.6189	43.9	(101)	SnO_2
	38.27	0.2434	2.3500	34.6	(200)	SnO_2
	39.30	0.1894	2.2909	44.6	(111)	SnO_2
	52.09	0.2435	1.7543	36.3	(211)	SnO_2

	55.07	0.2435	1.6663	36.8	(220)	SnO_2
	58.12	0.2975	1.5858	30.6	(002)	SnO_2
	62.24	0.2705	1.4905	34.3	(310)	SnO_2
	65.05	0.2976	1.4327	31.7	(112)	SnO_2
	66.29	0.2705	1.4088	35.1	(301)	SnO_2
5	26.91	0.2435	3.3109	33.6	(110)	SnO_2
	34.21	0.2164	2.6189	38.4	(101)	SnO_2
	38.30	0.2434	2.3484	34.6	(200)	SnO_2
	39.32	0.2975	2.2894	28.4	(111)	SnO_2
	52.09	0.2975	1.7543	29.7	(211)	SnO_2
	55.04	0.2705	1.6671	33.1	(220)	SnO_2
	58.18	0.3246	1.5844	28.0	(002)	SnO_2
	62.21	0.2976	1.4911	31.2	(310)	SnO_2
	65.02	0.2706	1.4332	34.8	(112)	SnO_2
	66.24	0.3246	1.4098	29.2	(301)	SnO_2
7	26.96	0.2164	3.3044	37.8	(110)	SnO_2
	33.32	0.2164	2.6870	38.3	(222)	Mn_2O_3
	34.27	0.2164	2.6149	38.4	(101)	SnO_2
	38.32	0.2705	2.3468	31.1	(200)	SnO_2
	39.35	0.2435	2.2879	34.7	(111)	SnO_2
	52.17	0.2164	1.7518	40.9	(211)	SnO_2
	55.15	0.2705	1.6641	33.1	(220)	SnO_2
	58.23	0.2705	1.5831	33.6	(002)	SnO_2
	62.26	0.2976	1.4899	31.2	(310)	SnO_2
	65.10	0.3246	1.4316	29.0	(112)	SnO_2
	66.35	0.2705	1.4078	35.1	(301)	SnO_2
9	23.39	0.1352	3.8001	60.0	(211)	Mn_2O_3
	26.85	0.2435	3.3174	33.6	(110)	SnO_2
	33.13	0.2165	2.7019	38.3	(222)	Mn_2O_3
	34.10	0.2164	2.6270	38.4	(101)	SnO_2
	38.21	0.2435	2.3532	34.5	(200)	SnO_2
	39.27	0.1894	2.2924	44.6	(111)	SnO_2
	52.01	0.2976	1.7568	29.7	(211)	SnO_2
	55.01	0.2164	1.6678	41.4	(220)	SnO_2
	58.10	0.2705	1.5864	33.6	(002)	SnO_2
	62.13	0.2976	1.4928	31.2	(310)	SnO_2
	65.00	0.3246	1.4337	29.0	(112)	SnO_2
	66.19	0.2705	1.4108	35.1	(301)	SnO_2

Table 2: The lattice constants as a function of Mn doping ratio.

Mn%	a (Å)	c (Å)
0	4.68230	3.17018
3	4.68230	3.17153
5	4.68230	3.16884
7	4.67307	3.16615
9	4.69155	3.17288

A.C Conductivity Spectra.

One useful technique for understanding the electrical characteristics of the manufactured composites is the ac conductivity approach. Figure 2 illustrates the fluctuation of conductivity with angular frequency of $(SnO_2)_{1-x}(Mn_2O_3)_x$ in the frequency range of 1 to 200 kHz at different doping ratios. At room temperature, the conductivity of $(SnO_2)_{1-x}(Mn_2O_3)_x$ composites was computed, regardless of temperature. Figure 2 shows that $\sigma_{ac}(\omega)$ grows exponentially with frequency across the whole frequency range, indicating pure ac conductivity and electronic polarization. The figure illustrates how the polarization of the space charge causes σ_{ac} to grow as the frequency increases [14]. Figure 2 shows that at high doping levels of Mn_2O_3 particles, the electrical conductivity (σ_{ac}) has a high value. The behavior of σ_{ac} with frequency can be explained by an increase in the number of charge carriers, which lowers resistivity and increases

According to Equation (4), $\sigma(\omega,T)$ α ω^s if $\sigma_{dc}(T)$ is less than is less than $a(T)\omega^s$ for a given temperature. As a result, the plot of ln (σ) vs ln(ω) represents a straight line with slope (s). Table (3) gives the values of (s) for $(SnO_2)_{1-x}(Mn_2O_3)_x$ composites. It can be noticed that (s) decreases with increase of doping ratio from 0 to 5%; hence correlated barrier hopping (CBH)is the suitable model. This model is adopted when the electrons hop over the potential barrier between two sites; the ac conductivity is due to hopping between defect states or dangling bonds (D +D−). The conductivity here is pure ac since $\sigma_{ac}(\omega)$ is exponentially dependent on frequency, and the exponent (s) exceeds unity [18].
On the other hand, increases with the increase of Mn content for high doping ratio i.e. 7% and 9% which makes the small polaron (SP) the most suitable model. When the exponent s gets to increase with the increase of Mn content, this indicates that the covalent solid has received an excess charge carrier, which causes a significant degree of lattice deformation and the production of a small polaron [19-22].

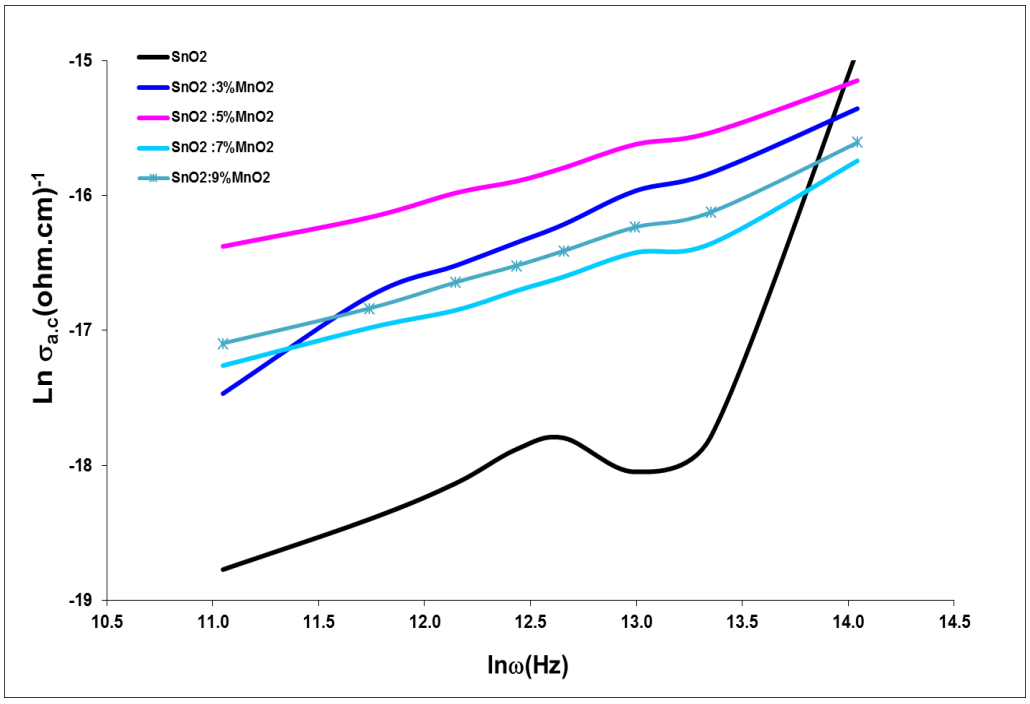

Figure 2: Conductivity curves of $(SnO_2)_{1-x}(Mn_2O_3)x$ for different doping ratios.

Cole-Cole plots

Using an LCR meter, the dielectric characteristics of the $(SnO_2)_{1-x}(Mn_2O_3)_x$ composites were evaluated. In the frequency range of 10 to 200 kHz, the resistance, capacitance, and loss factor were measured using the LCR meter. The real dielectric constant (ε_1) was plotted against the imaginary dielectric constants (ε_2) in a Cole-Cole plot.

The Cole-Cole plots of $(SnO_2)_{1-x}(Mn_2O_3)_x$ composite samples at different doping ratios are displayed in Figure 3. The plots showed a straight diagonal line in the low-frequency domain. A partially semicircular arc was in the high-frequency region after a single peak in the low-frequency region that provided information on the impact of blocking electrodes [23]. The real dielectric constant axis was above the semicircle's center [24]. Semicircles were partially visible on the high-frequency side, representing the electrode's reaction. The grain border area and the low-frequency semicircle were connected, with the former coming from the grain interior region [23].

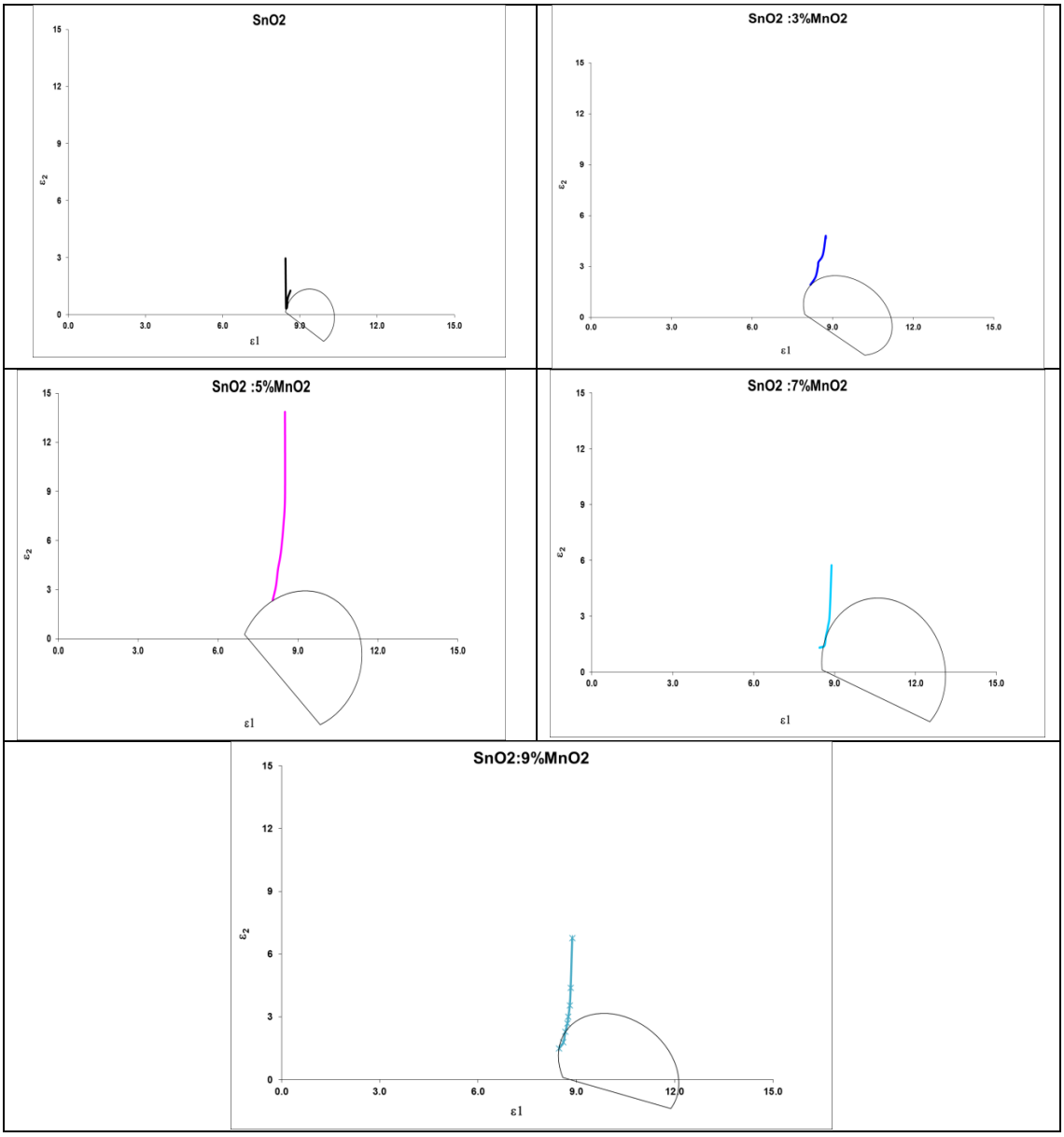

Figure 3: Cole-Cole plots of $(SnO_2)_{1-x}(Mn_2O_3)x$ for different doping ratios.

The polarizability (α) was calculated according to $\theta=\alpha\pi/2$ where θ is the diagonal angle below the dielectric constant axis, as listed in Table 3.

Dielectric Spectra

The variation of ε_1 and ε_2 of the $(SnO_2)_{1-x}(Mn_2O_3)_x$ composites with frequency is shown in Figures 4 and 5. It is evident from the figures that ε_1 and ε_2 values are large at low frequencies. This indicates that the dipoles have enough time in this region to orient themselves in the direction of the electric field. Additionally, the impact of electrical polarization (space charge polarization) causes charge carriers to accumulate at the electrode-composite interface. The values of ε_1 and ε_2 decreased with the exponential increase of frequency and reached a fixed value. This variation in the dielectric characteristics can be attributed to the fact that more ions do not propagate in the direction of the electric field, and, as a result, the polarization of the space charge decreases with increasing frequency [24]. As a result, the charge carriers contribute less to the dielectric properties as displayed in Figures 4 and 5.

For more explanation, it is obvious that ε_1 tends to decrease with increasing frequency to reach lower values. This can be ascribed to the fact that the electrode blocking layer is dominated; thus, the dielectric behavior is affected by the electrode polarization, while at high frequency the dielectric signal is not affected by electrode polarization.

As noted from the figures, ε_1 and ε_2 of SnO_2 increased with the increase in the concentration of (Mn_2O_3); this behavior is ascribed to more addition of free charge carriers [25,26].

From the relation of (ε_1) versus log ω, it is evident that (ε_1) values are affected greatly by the doping ratio; at a frequency of 1kHz, ε_1 increased from 86.26 to 87.46 as Mn was added to the SnO_2 lattice when the doping ratio increases from 0 to % 3. It decreased at 7% doping ratio to increase again to 88.72 at 9% doping ratio. The reason behind the increase in the value of ε_1 is the creation of a non-linear capacitor or conductor. Additionally, the migration of charge carriers or the trapping and buildup of charge carriers at interfaces and flaws cause the distortion of the electric field. The Maxwell-Wagner effect is the name given to this kind of polarization, which depends on the conductivity of the current phases [27].

Conversely, as the frequency increased, ε_1 fell to lower values. This can be explained by the electrode blocking layer's dominance, which causes the electrode polarization to have an impact on the dielectric behavior at low frequencies but not the dielectric signal at high frequencies [28]. (ε_2) versus ln (ω) is shown in Figure 5 for $(SnO_2)_{1-x}(Mn_2O_3)_x$ composites with different doping ratios. According to Deby's intrinsic relaxation time, ε_2 versus ln (ω) of $(SnO_2)_{1-x}(Mn_2O_3)_x$ predicts that these curves must be symmetrical around ω_D, which is the angular frequency (ω_D) corresponding to maximum absorption (an absorption peak), according to the equation $(\omega_D= 1/\tau)$, where τ represents the most probable value of a spread of relaxation times. Figure 5 clearly shows that a high Mn_2O_3 doping ratio caused the absorption peak to move into a lower frequency band. The calculated relaxation time (τ) is shown in Table 3. It is evident that when the doping ratio increases, (τ) values drop; this suggests that an increase in doping ratio increases the intermolecular force. The composite samples become more conductive, as indicated by the decrease in relaxation time. As was previously mentioned, there is a strong correlation between electrical conductivity and dielectric relaxation time. There are some parameters like relaxation time which give indication for how long a semiconductor must be neutralized during conduction. Therefore, the relaxation time is considerable in semiconductors and insulators and small in metals [29]. It must be noted that the dielectric loss values are very high; therefore, the large loss of energy stored within the dielectric material is also high.

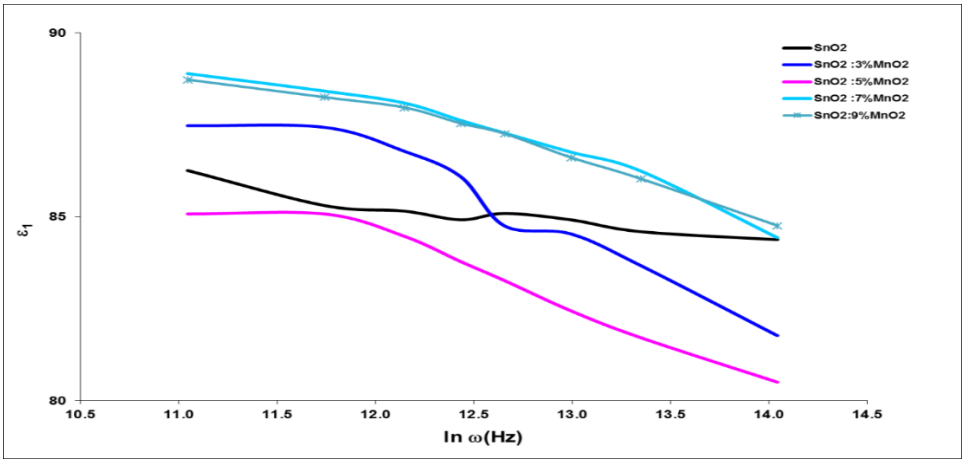

Figure 4: Real dielectric constant ε_1 of $(SnO_2)_{1-x}(Mn_2O_3)x$ as a function of logarithm ω for different doping ratios

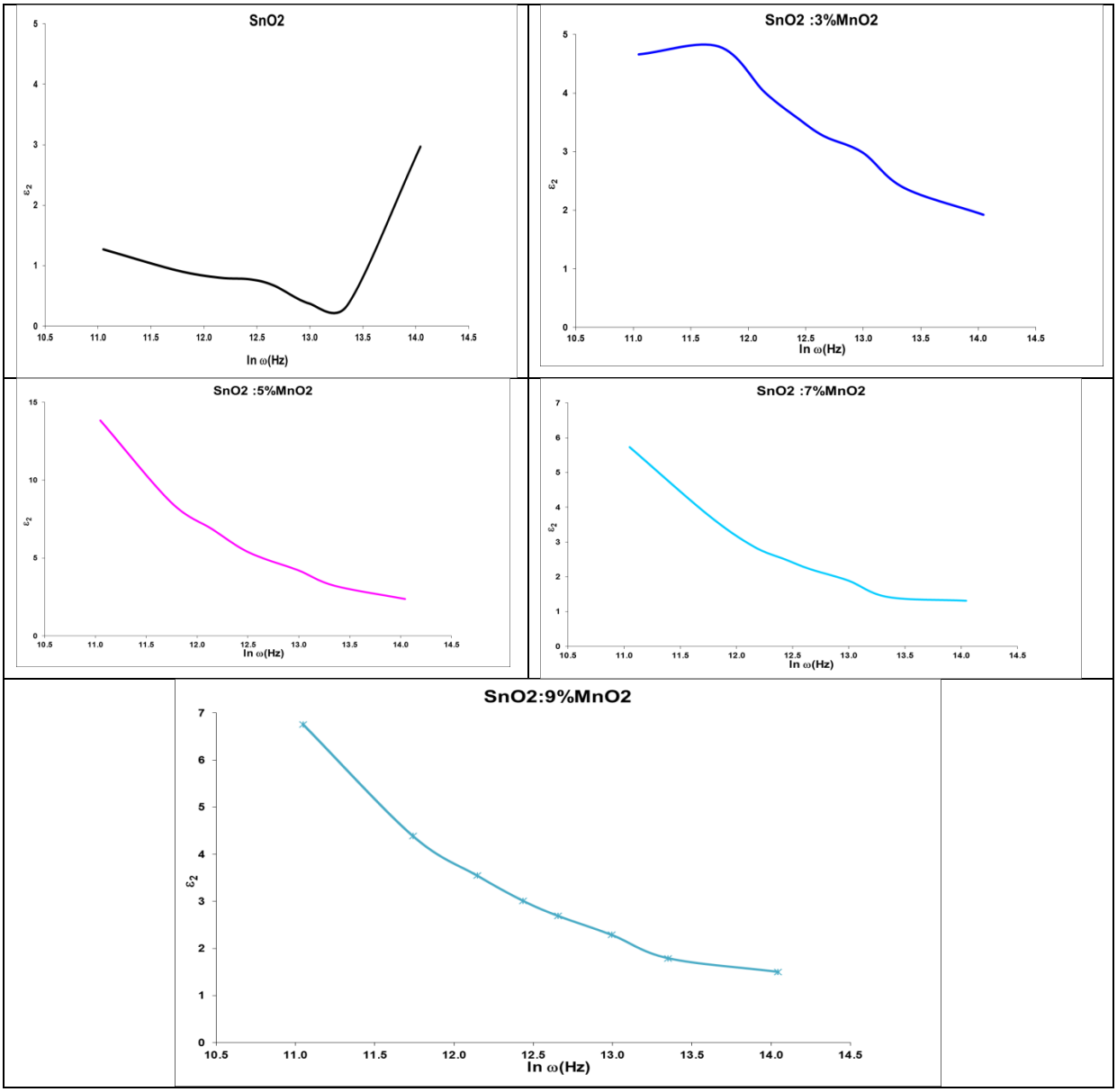

Figure 5: Imaginary dielectric constant ε_2 of $(SnO_2)_{1-x}(Mn_2O_3)_x$ as a function of logarithm ω

for different doping ratios.

Table 3: The polarizability (α) values.

Sample	s	α	τx10^{-6}
SnO_2	1.0176	0.333333333	3.18
SnO_2 :3%Mn_2O_3	0.6721	0.288888889	7.96
SnO_2 :5%Mn_2O_3	0.4072	0.466666667	3.98
SnO_2 :7%Mn_2O_3	0.4811	0.333333333	2.27
SnO_2 :9%Mn_2O_3	0.4850	0.122222222	2.27

Conclusions

Solid-state reaction technology was used to create tin oxide pellets doped with manganese. The produced samples with tetragonal structure were polycrystalline, as found the X-ray diffractogram. Mn ions replacement in the SnO_2 lattice was confirmed by the XRD pattern of the pellets, as seen by the peak shift of the SnO_2 diffraction plane. Using the XRD method, the crystalline size and lattice characteristics were found. Using the Debye-Scherer formula, the film's crystalline size was determined to be between 33.6 and 37.8 nm. The lattice constants were a = 4.68-3.69 and c = 3.166-3.17-3. This study also reports the electrical properties of the manufactured composite samples.

References

[1] J. Liu, Y. Zhang, J. Qi, Y. Huang, X. Zhang, and Q. Liao, "In-doped zinc oxide dodecagonal nanometer thick disks," *Materials Letters*, vol. 60, no. 21-22, pp. 2623-2626, 2006.

[2] B. Liu, C. W. Cheng, R. Chen, Z. X. Shen, H. J. Fan, and H. D. Sun, "Fine structure of ultraviolet photoluminescence of tin oxide nanowires," *The Journal of Physical Chemistry*, vol. 114, no. 8, pp. 3407-3410, 2010.

[3] R. Viswanatha, S. Sapra, S. Sen Gupta, B. Satpati, P. V. Satyam, B. N. Dev, and D. D. Sarma., "Synthesis and characterization of Mn-doped ZnO nanocrystals," *The Journal of Physical Chemistry B*, vol. 108, no. 20, pp. 6303-6310, 2004.

[4] P. Sharma, A. Gupta, F. J. Owens, A. Inoue, and K. V. Rao, "Room temperature spintronic material—Mn-doped ZnO revisited," *Journal of Magnetism and Magnetic materials*, vol. 282, pp. 115-121, 2004.

[5] Y. S. Wang, P. J. Thomas, and P. O'Brien., "Optical properties of ZnO nanocrystals doped with Cd, Mg, Mn, and Fe ions," *The Journal of Physical Chemistry B*, vol. 110, no. 43, pp. 21412-21415, 2006.

[6] X. G. Chen, W. W. Li, J. D. Wu, J. Sun, K. Jiang, Z. G. Hu, and J. H. Chu., "Temperature dependence of electronic band transition in Mn-doped SnO2 nanocrystalline films determined by ultraviolet-near-infrared transmittance spectra," *Materials Research Bulletin*, vol. 47, no. 1, pp. 111-116, 2012.

[7] F. Gu, S. F. Wang, C. F. Song, M. K. Lü, Y. X. Qi, G. J. Zhou, D. Xu, and D. R. Yuan., "Synthesis and luminescence properties of SnO2 nanoparticles," *Chemical Physics Letters*, vol. 372, no. 3-4, pp. 451-454, 2003.

[8] E. L. Papadopoulou, M. Varda, K. Kouroupis-Agalou, M. Androulidaki, E. Chikoidze, P. Galtier, G. Huyberechts, and E. Aperathitis, "Undoped and Al-doped ZnO films with tuned properties grown by pulsed laser deposition," *Thin Solid Films*, vol. 516, no. 22, pp. 8141-8145, 2008.

[9] E. Kumar, S. C. Velladurai, L. Guru Prasad, D. Muthuraj, and V. Bena Jothy., "Preparation and investigation on structural, spectral and electrical properties of polyaniline/manganese dioxide nanocomposites," *J. Mater. Environ. Sci*., vol. 8, no. 10, pp. 3490-3495, 2017.

[10] Abdel-karim, Amal M., A. H. Salama, and Mohammad L. Hassan. "Electrical conductivity and dielectric properties of nanofibrillated cellulose thin films from bagasse." Journal of Physical Organic Chemistry ,Vol.31, no. 9, 2018.

[11] Z. M. Tian, S. L. Yuan, J. H. He, P. Li, S. Q. Zhang, C. H. Wang, Y. Q. Wang, S. Y. Yin, and L. Liu, "Structure and magnetic properties in Mn doped SnO2 nanoparticles synthesized by

chemical co-precipitation method," *Journal of Alloys and Compounds*, vol. 466, no. 1-2, pp. 26-30, 2008.

[12] N. S. Sabri, M. K. Talari, and A. K. Yahya, "Structural and Optical Properties: Mn Doped Nano ZnO Synthesized by Mechanochemical Synthesis," *In AIP Conference Proceedings*, vol. 1250, no. 1, pp. 436-439, 2010.

[13] B. Sathyaseelan, K. Senthilnathan, T. Alagesan, R. Jayavel, and K. Sivakumar, "A study on structural and optical properties of Mn-and Co-doped SnO2 nano crystallites," *Materials Chemistry and Physics*, vol. 124, no. 2-3, pp. 1046-1050, 2010.

[14] X. Huang, Z. Yu, Shuqing Huang, Q. Zhang, D. Li, Y. Luo, and Q. Meng, "Preparation of fluorine-doped tin oxide (SnO_2: F) film on polyethylene terephthalate (PET) substrate," *Materials letters*, vol. 64, no. 15, pp.1701-1703, 2010.

[15] A. Hashim, M. A. Habeeb, A. Khalaf, and A. Hadi, "Fabrication of (PVA-PAA) Blend Extracts of Plants Bio-Composites and Studying Their Structural, Electrical and Optical Properties for Humidity Sensors Applications," *Sensor Letters*, vol. 15, no. 7, PP. 589–596, 2017.

[16] K. J. Kadhim, I. R. Agool, and A. Hashim, "Effect of zirconium oxide nanoparticles on dielectric properties of (PVA-PEG-PVP) blend for medical application," *Journal of Advanced Physics*, vol. 6, no. 2, pp: .187-190, 2017.

[17] B. A. Hasan, and D. A. Umran, "Dielectric permittivity and ac conductivity of CuInSeTe thin films," *Semiconductor Science and Technology*, vol. 27, no. 12, pp. 125014, 2012.

[18] A. R. Von Hipped, "Dielectric and Wave" Wiley, London, (1954)

[19] H. A. Pohl, and R. Pethig, "Dielectric measurements using non-uniform electric field (dielectrophoretic) effects," *Journal of Physics E: Scientific Instruments*, vol. 10, no. 2, p. 190, 1977.

[20] A. A. Hasan, "Dielectric Study of PVC-LiF Composites Films," *Iraqi Journal of Science*, vol. 62, no. 3, pp.861-870, 2021.

[21] Soltan, Wissem Ben, Saber Nasri, Mohamed Saber Lassoued, and Salah Ammar. "Structural, optical properties, impedance spectroscopy studies and electrical conductivity of SnO_2 nanoparticles prepared by polyol method." Journal of Materials Science: Materials in Electronics 28, no. 9, pp. 6649-6656, 2017.

[22] B. A. Hasan, H. H. Issa and A. A. Hasan, "Fabrication and Investigation of Structural, Optical and Dielectric Properties of ZnO: MnO_2Composites," *Iraqi journal of applied physics*, vol. 19, no. 4A, pp. 21-28, 2023.

[23] S. Hegde, V. Ravindrachary, S.D. Praveena, B. Guruswamy, R.N. Sagar, "Optical and dielectric properties of Li + ion conducting solid polymer electrolyte," *Indian J. Adv. Chem. Sci*., vol. 13, no. 1, pp. 83-87, 2018.

[24] C. H. Hong, B. J. Park, and H. J. Choi, "Comment on "Electrorheological behavior of copper phthalocyanine-doped mesoporous TiO2 suspensions," *Journal of colloid and interface science*, vol. 300, no. 2, pp. 818-819, 2006.

[25] A. Hashim, and A. Hadi, "A novel piezoelectric material prepared from (carboxymethyl cellulose-starch) blend-metal oxide nanocomposites," *Sensor Letters*, vol. 15, no. 12, pp. 1019-1022, 2017.

[26] A. Hashim, A. Hadi, "Novel Pressure Sensors Made from Nanocomposites (Biodegradable Polymers–Metal Oxide Nanoparticles): Fabrication and Characterization," *Ukrainian Journal of Physics*, vol. 63, no. 8, p. 754, 2018.

[27] C. Li, G. Chen, X. Qiu, Q. Lou, and X. Gao, "A direct proof for Maxwell–Wagner effect of heterogeneous interface, " *AIP Advances*, vol. 11, no. 6, p. 065227, 2021.

[28] K. Auromun, S. Hajra, R.N.P. Choudhary, and B. Behera, " Structural, dielectric and electrical characteristics of yttrium modified $0.7BiFeO_3$-$0.3PbTiO_3$," *Solid State Sciences*, vol. 101, p. 106139, 2020.

[29] J, K. McCusker, "Electronic structure in the transition metal block and its implications for light harvesting," *Science*, vol. 363, no. 6426, pp. 484-488, 2019.